Received 10 December 2019; revised 14 January 2020; accepted 29 January 2020. Date of publication 3 March 2020; date of current version 13 March 2020.

Digital Object Identifier 10.1109/OJAP.2020.2977662

Triple-Band Reconfigurable Low-Profile Monopolar Antenna With Independent Tunability

KEN PARAMAYUDHA [1,2], SHENGJIAN JAMMY CHEN [1] (Member, IEEE), THOMAS KAUFMANN [1,3] (Member, IEEE), WITHAWAT WITHAYACHUMNANKUL [1] (Senior Member, IEEE), AND CHRISTOPHE FUMEAUX [1] (Fellow, IEEE)

[1]School of Electrical and Electronic Engineering, University of Adelaide, Adelaide, SA 5005, Australia

[2]Research Center for Electronics and Telecommunication, Indonesian Institute of Sciences (PPET-LIPI) 40135, Bandung, Indonesia

[3]u-blox AG, Technology Positioning, 8800 Thalwil, Switzerland

CORRESPONDING AUTHOR: K. PARAMAYUDHA (e-mail: ken.paramayudha@lipi.go.id)

ABSTRACT This article proposes a reconfigurable low-profile monopolar antenna with triple-band independent tuning capability. The antenna is based on the concept of a center-fed patch with shortings to achieve omnidirectional radiation patterns. Instead of using vias, varactor-loaded stubs are utilized to create reconfigurable equivalent shorting points. The triple bands can be achieved by using three sets of stubs. This configuration results in three magnetic current loops that spatially overlap at different independently tunable frequencies. Measurement results show that the design obtains three independent tunable frequencies centered at 2.51, 3.56, and 4.62 GHz with −10 dB relative tuning ranges of 22.8%, 22.8%, and 16.7%, respectively. The antenna radiates omnidirectionally with vertical polarization in the three sweeping bands. The proposed concept can be extended to a larger number of bands by adding sets of stubs with considerations of coupling and impedance matching.

INDEX TERMS Triple-band, frequency-reconfigurable, low-profile, monopole, patch antennas.

I. INTRODUCTION

IN RECENT decades, the demand in wireless communications has risen significantly. This has brought upon increasing congestion of the available radio spectrum. Therefore, it is desirable to have antennas that can cover several allocated frequency bands simultaneously. To accomplish the goal, wideband antennas with a low-profile monopole structure are often desired due to their omnidirectionality, low-cost, and fabrication simplicity [1]–[5]. Another solution is to use frequency-agile antennas that have been widely developed recently. Compared to wideband antennas, a frequency-reconfigurable antenna can mitigate undesirable interference from unused bands, thus ease requirements on additional RF filters in the system.

Frequency-reconfigurability can be obtained by modifying the antennas electrical properties with the assistance of active elements such as PIN diodes [6]–[8], RF-MEMS switches [9]–[11], varactor diodes [12]–[16], or their combinations [17], [18]. In [6], PIN diodes were used in the slot of a planar monopole ground plane to switch the antenna states into a single-band, dual-band, or ultrawideband, whereas in [9], an RF-MEMS switch was utilized in the slot of a patch antenna to switch the operation frequency. In varactor-loaded antennas, varying the bias voltage leads to a progressive variation in the diode capacitance that can create a continuous frequency tuning. Because of this feature, adopting varactors to create frequency-reconfigurable antennas is beneficial, in particular for applications that require a large number of operating bands with continuous tunability.

Numerous concepts of antennas with continuous frequency tunability have been previously proposed in the literature. The structures used for the antennas were shorted patches [13], [15], [16], slotted patches [12], [19]–[25], dipoles [26]–[28], planar inverted-F antennas (PIFA) [29], half-mode substrate integrated waveguides (HMSIW) [30], [31], multi radiators [17], [18], and low-profile monopoles [14], [32]–[34]. Nonetheless, only a few of those proposed antenna designs are able to cover more

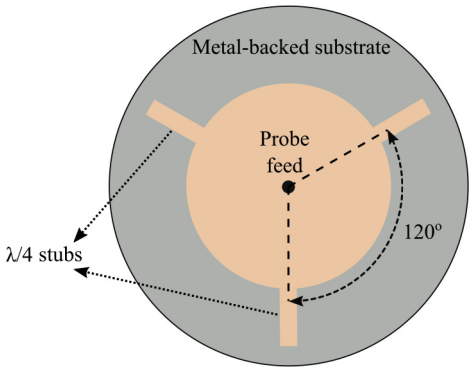

FIGURE 1. Basic geometry of a single-band low-profile monopole antenna with stubs for shorting. The figure shows the top view, where the ground plane is hidden.

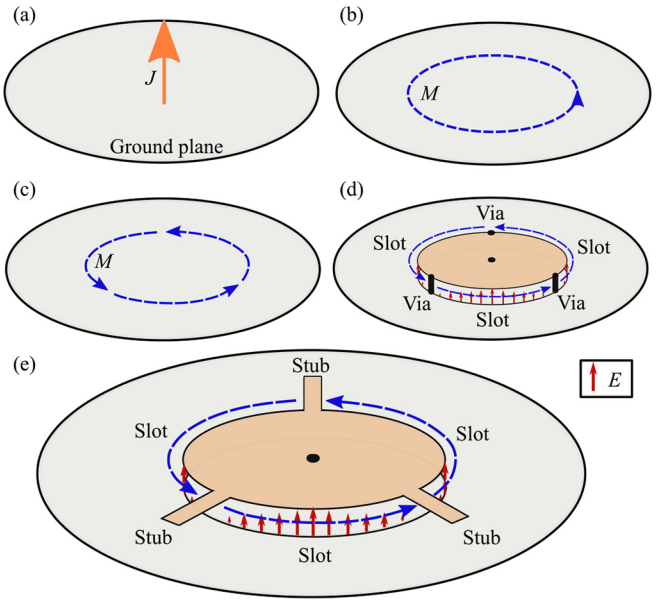

FIGURE 2. Operation principle of the proposed low-profile monopole antenna based on magnetic current loop. (a) Electric current and (b) its equivalent magnetic current loop, (c) discretization of magnetic currents, (d) realization in a center-fed patch with vias, and (e) with quarter-wave open stubs.

than one band at the same time [12], [14], [21], [22], [24], [25], [34]. In the case of multi-band reconfigurable antennas, the independency of frequency sweeping is one desirable feature. Behdad and Sarabandi [12] demonstrated a broadside-pattern dual-band reconfigurable antenna with independent tuning of the bands. This was obtained by loading varactors onto a bent slot antenna. Recently, an antenna with tri-band independent tuning capability was presented by Bai *et al.* [25]. In this case, the design was specific for radio receivers with broadside radiation patterns and only −6 dB reflection coefficient. For low-profile monopole antennas, the independent tunability of two frequencies was reported by Nguyen-Trong *et al.* [14]. For that dual-band design, stable omnidirectional patterns were achieved in all sweeping frequencies with relative tuning ranges of 31% and 22% in the first and the second bands.

In this paper, a triple-band frequency-reconfigurable low-profile monopolar antenna is proposed based on the concept of independent magnetic current loops sharing a common thin aperture. The antenna is composed of a center-fed circular patch with three groups of stubs located on the patch edge. Each set of stubs functions as equivalent shortings at a particular frequency to define a magnetic current loop at the perimeter of the patch [35], [36]. To achieve a continuous frequency reconfigurability, varactor diodes are placed between the patch and the stubs. These varactors are biased with three DC control voltages to tune the three frequencies independently. Monopolar radiation patterns with reasonable azimuthal variations are obtained across the three tuning ranges.

This article will begin with an explanation on the operation principle of the antenna. In particular this includes an illustration of magnetic current loops that will play an important role in the multi-band radiation. Then, the concept of reconfigurability will be validated with a triple-band reconfigurable design, followed by concluding remarks.

II. OPERATION PRINCIPLE

As shown in Fig. 1, the basic geometry of the single-band low-profile monopole antenna consists of a center-fed circular patch on a substrate with a ground plane underneath. The patch is surrounded by three stubs on its edge with 120° angular separation. The radiation principle of the antenna is based on the magnetic current loop formed by a low-profile shorted monopole antenna, as discussed in [35]. As shown in Fig. 2(a), we begin with a vertical electric current with density J that is equivalent to a magnetic current loop with constant density distribution M depicted in Fig. 2(b), both placed over a ground plane. The magnetic current loop M can be established with three in-phase magnetic current elements as shown in Fig. 2(c), which in theory can be realized from thin slots in a metallic cavity. For a substrate integrated design, such a slot aperture can be created between two adjacent vias shunting the top patch with the ground, as shown in Fig. 2(d). The substrate thickness should be sufficiently small so that a purely transverse electric field E is present in the slots. On resonance, each of these slots can be considered as a $\lambda/2$ transmission line (slot line) that is shorted at its two ends. As a result, three slot apertures are formed between three shorts, with the highest E-field magnitude occuring in the middle of the slots. Furthermore, as has been demonstrated in [36], [37], vias can be replaced by quarter-wavelength stubs as shown in Fig. 2(e). It is noted that for this antenna configuration, the slot and the stub lengths influence the effective size of the cavity and thus the resonance frequency [36].

To open a second band, an additional set of three shorting stubs with a specific length determined by the targeted frequency can be interlaced with the original set. This basically defines two sets of slots that radiate at different frequencies. A preliminary simulation of this concept has been carried out in CST Microwave Studio with the results shown in Fig. 3. The base antenna is designed with a diameter of 36 mm, whereas the lengths of the longer and

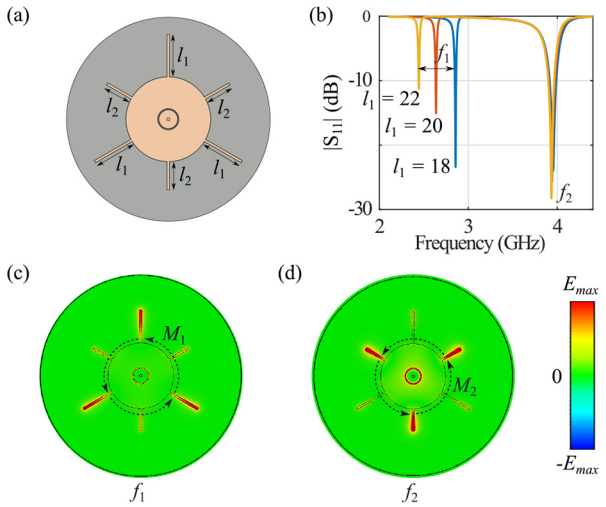

FIGURE 3. Dual-band low-profile monopole with stub shortings. (a) Antenna geometry, (b) reflection coefficient of the antenna when $l_1 = 18$, 20, and 22 mm, and (c,d) instantaneous *E*-field in the substrate at resonance frequencies of f_1 and f_2.

shorter stubs are $l_1 = 20$ mm and $l_2 = 16$ mm, respectively. Dual-band performance is then observed in the frequencies of around $f_1 = 2.8$ GHz and $f_2 = 3.9$ GHz. The longer stubs are responsible for the lower operation frequency f_1 as indicated in the *E*-field simulation shown in Fig. 3(c). In contrast, the three shorter stubs are responsible for the resonance at the higher frequency f_2 as illustrated in Fig. 3(d). It is important to note that in this structure, the two sets of magnetic current elements M_1 and M_2 work independently. This concept is further supported by the parametric simulation depicted in Fig. 3(b). In this scenario, the variation of the stub length l_1 shifts the resonance frequency f_1 while f_2 remains nearly unchanged. This scenario also implies that the center frequency of the bands can be adapted to specifications by changing the corresponding stub lengths. Furthermore, the concept is generic and can potentially be extended to more bands by adding additional sets of stubs. In this article, the extension of the principle into a triple-band device will be demonstrated.

Instead of varying the stub length, the resonance frequencies of the multi-band antenna can be tuned independently by varying the stub impedance, which can be implemented by integration of varactor diodes [31]. Separate sets of varactors are placed between the patch edge and the stubs to control the current flows. As a result, changing the capacitance of one set of varactors can shift the frequency in one band while the other band remains unaffected. In addition, it is worth mentioning that the monopolar radiation pattern with vertical polarization is expected to be maintained in all bands as the magnetic current slots remain the predominant radiating sources.

III. TRIPLE-BAND RECONFIGURABLE DESIGN

A. ANTENNA GEOMETRY

The design and the photographs of the fabricated antenna are depicted in Fig. 4 and Fig. 5. This triple-band reconfigurable

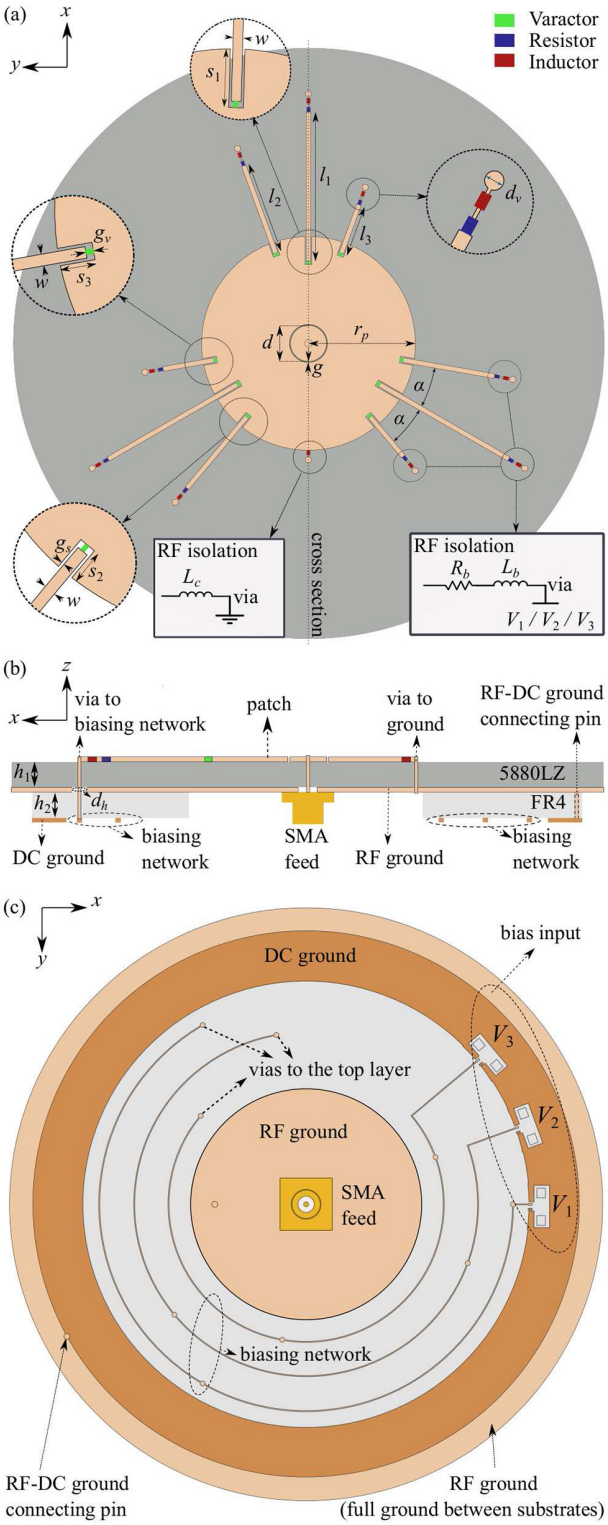

FIGURE 4. Triple-band reconfigurable antenna design. (a) Top, (b) cross-sectional, and (c) bottom views. Dark grey color is the 5880LZ substrate, light grey color is the FR-4 substrate, light brown color is copper on 5880LZ substrate, and dark brown color is copper on FR-4 substrate. The dimensions (mm) are: $l_1 = 32$, $l_2 = 20$, $l_3 = 11$, $s_1 = 6$, $s_2 = 3$, $s_3 = 3$, $w = 1$, $d = 8$, $r_p = 23$, $g = 0.1$, $g_V = 0.66$, $g_S = 0.25$, $d_V = 0.9$, $d_h = 1.8$, $h_1 = 4.32$, and $h_2 = 1.6$.

design is created on Rogers Duroid 5880LZ substrate with a relative permittivity of $\epsilon_r = 2.0$ and a loss tangent of $\tan\delta = 0.0027$. The thickness of the substrate h_1 is chosen to be

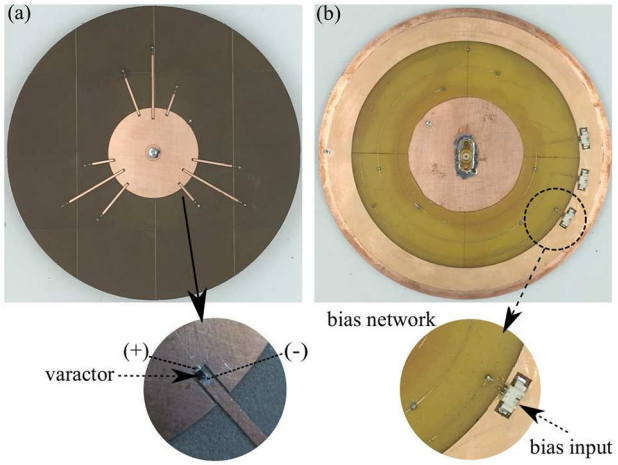

FIGURE 5. Fabricated antenna. (a) Top and (b) bottom views.

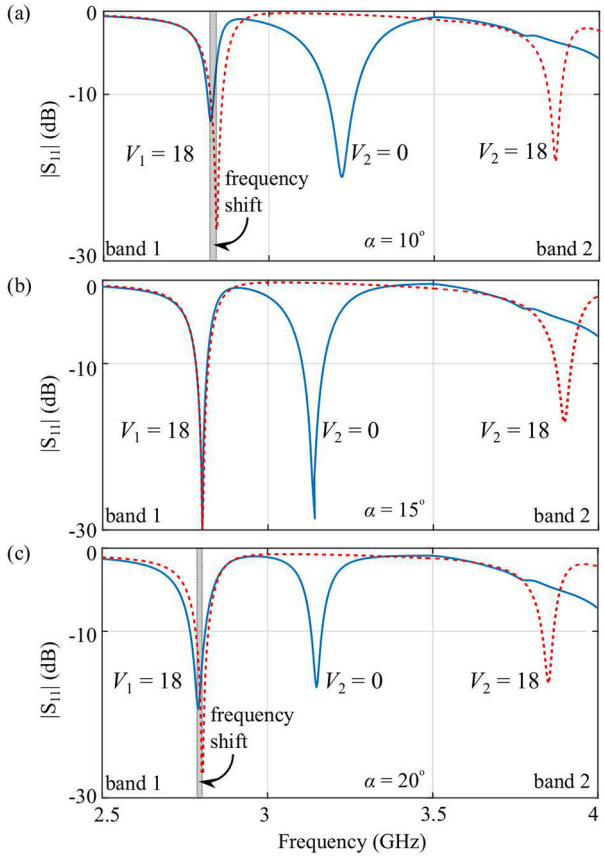

FIGURE 6. Reflection coefficients of the antenna at the first and the second bands with consecutive stub angles α of (a) 10°, (b) 15°, and (c) 20°. The voltage of the first band V_1 is fixed at 18 V and the voltage of the second band V_2 is tuned to the minimum and the maximum of 0 V and 18 V.

4.32 mm (or about $0.032\lambda_{\min}$). A thick substrate is required to attain good impedance matching in each of the three bands and to improve the radiation efficiency. Nine stubs divided into three sets of different lengths are utilized to introduce three shorting conditions at three particular frequencies. The width of these stubs should be sufficiently narrow so that the stubs do not radiate. For that reason, a stub width $w = 1$ mm is used in the design. The center pin as a probe feeding is created from a 50-Ω SMA connector through the ground plane. The ground plane is circular for symmetry with a diameter of 150 mm. The bias network is implemented on another layer below the full RF ground plane using an FR-4 substrate with a thickness h_2 of 1.6 mm. Separating the DC circuitry from the RF board avoids the effect of bias lines that can disturb the radiation pattern of the antenna.

Based on our investigation, a larger number of stubs is found to increase mutual coupling effects, which in turn affect the tuning independence. The coupling is not only between adjacent stubs but also between the inactive stubs and the active radiating slots. It is known from a typical slot antenna that the highest amplitude of the E-field occurs in the middle of the slot when it resonates in its fundamental mode. Because of this, it is advisable to avoid placing inactive stubs close to the middle of an active radiating slot. A parametric optimization of the design has been carried out to balance trade-offs between stub-to-stub and stub-to-slot coupling, as illustrated in Fig. 6. Figure 6(a), (b), and (c) show the reflection coefficients of the antenna at the first and the second bands with adjacent stub angles α of 10°, 15°, and 20°, respectively. In these scenarios, the voltage of the first band is fixed at 18 V and the voltage of the second band is tuned to the minimum and the maximum of 0 V and 18 V. It can be seen from Fig. 6(a) and (c) that there is a slight frequency shift of approximately 0.9% and 0.5% for the first band when α is set to be 10° and 20°, respectively. Meanwhile, it can be said that there is no frequency shift when $\alpha = 15°$, as illustrated in Fig. 6(b). Therefore, an optimal angle between the consecutive stubs is found to be 15°.

For impedance matching purpose, the capacitive gap around the probe and the recesses around the stubs are created and optimized. The probe cap with a diameter of d can be seen as a radial inductor whereas the circular ring gap g adds the capacitance as explained in [1]. The recess configuration for the stubs is adopted from the well-known impedance matching technique for patch antenna feeding [38]. The depths of the recesses are shown in Fig. 4 as s_1, s_2, and s_3.

B. BIAS CIRCUIT

The varactors used in the design are MA46H120 from MACOM Technical Solutions. The capacitance of this type of varactor ranges from 1.30 to 0.15 pF when reverse-biased at 0 to 18 V [31]. The varactor internal resistance is approximately $R_v = 2$ Ω, and varies with the bias voltages as explained in [39]. These varactors are divided into three sets, one for each group of same-length stubs. These three varactor sets are biased separately by DC voltages V_1, V_2, and V_3 which are applied from the bottom layer through vias. A 1 MΩ resistor followed by an inductor is located after each stub as the RF choke. The inductors are

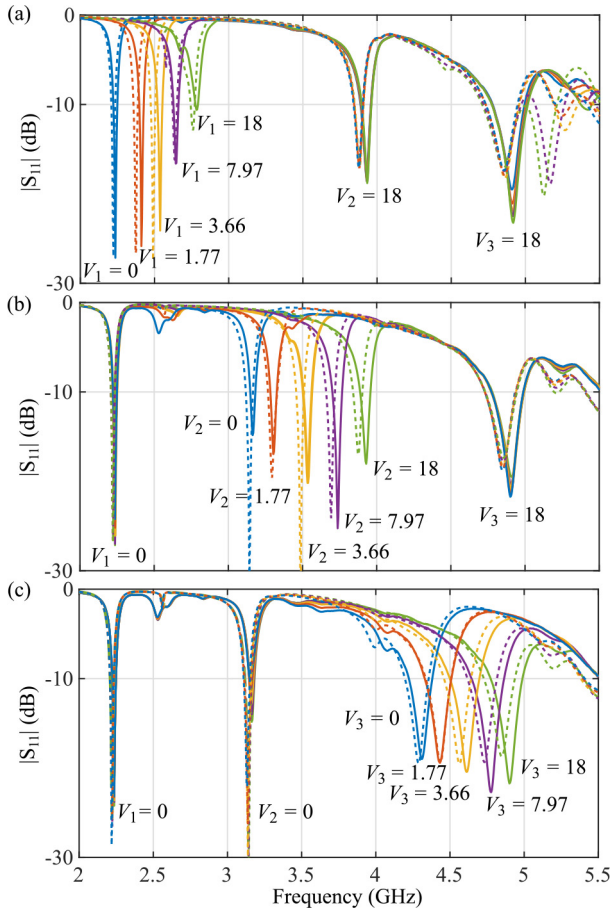

FIGURE 7. Measured (solid lines) and simulated (dotted lines) reflection coefficients of the triple-band reconfigurable low-profile monopole design for (a) varying the first band (V_1), (b) varying the second band (V_2), and (c) varying the third band (V_3). The unit for the voltages is Volt.

$L_b = 100$ nH for the shortest and the longest stub and $L_b = 24$ nH for the middle-length stubs. The value of inductors for the middle-length stubs is empirically chosen to suppress a spurious resonance. These two inductors are found appropriate taking into account their self resonant frequency (SRF). In addition to impedance matching, the capacitive gap at the feed blocks the DC current from flowing to the probe. A single via together with an RF choke $L_c = 100$ nH is used to DC-ground the circular patch. A full RF ground plane is used between the two substrates. The DC and RF-grounds are connected with a soldered pin as shown in Fig. 4(b) and (c). To allow the vias connecting the patch to the biasing network layer, circular holes with diameter $d_h = 1.8$ mm (about $0.013\lambda_{\min}$) are created on the RF ground plane. The size of these holes is set to be sufficiently small to avoid a detrimental effect on the radiation patterns of the antenna.

C. REFLECTION COEFFICIENT

Measured and simulated reflection coefficients with different bias voltages V_1, V_2, and V_3 agree well, as shown in Fig. 7. The three bands are centered at 2.51, 3.56, and 4.62 GHz.

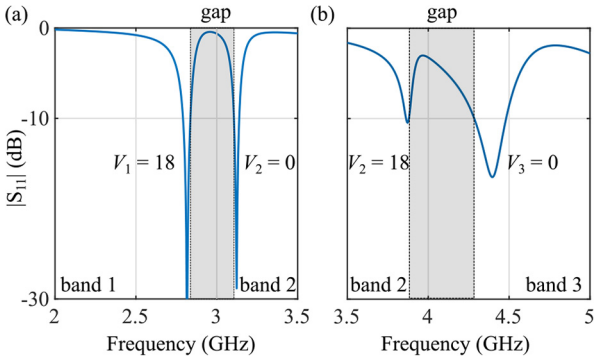

FIGURE 8. Reflection coefficients when the tuned resonances are close to each other. (a) First band is tuned with the maximum bias $V_1 = 18$ V and second band is tuned with the minimum bias $V_2 = 0$ V. (b) Second band is tuned with maximum bias $V_2 = 18$ V and third band is tuned with the minimum bias $V_3 = 0$ V.

In each scenario, only one band is tuned while the other two are fixed. It can be seen from all the scenarios that the tuning of one band does not affect the operation frequencies of the other two, with only a small effect on the impedance matching. Hence, the independence of frequency tuning is achieved for this triple-band antenna design. The measured -10 dB tuning ranges are 22.8% for the first band (2.22–2.79 GHz), 22.8% for the second band (3.15–3.96 GHz), and 16.7% for the third band (4.23–5.00 GHz). It is observed that additional out-of-band resonances occur at above 5 GHz. These resonances are related to the SRF of the RLC components for the RF blocker. An instantaneous impedance bandwidth of about 1% is obtained in the first band, 1% to 2% in the second band, and around 4% in the third band. This narrow-band feature is typical for multi-band reconfigurable antennas [12], [14], [21], [22], [24], [25], [34]. Nevertheless, with the wide and continuous frequency tuning capability, this antenna can cover a large operation bandwidth with an excellent frequency selectivity and remains low-profile owing to the narrow-band feature. This characteristic is highly desirable for applications such as cognitive radio.

Figure 8 shows two scenarios when the tuned resonances are close to each other. In the first scenario, the first band is tuned to the maximum bias voltage $V_1 = 18$ V and the second band is tuned to the minimum voltage $V_2 = 0$ V. For the second scenario, the second band is at the highest tuning voltage $V_2 = 18$ V and the third band at the lowest tuning voltage $V_3 = 0$ V. It is observed from the two scenarios that the antenna still maintains a satisfactory impedance matching with reflection coefficient below -10 dB. It is also noticed that there are separations of 360 MHz and 270 MHz between the first-second bands and the second-third bands, respectively. In these two scenarios of Fig. 8, the predominant radiating sources are still the magnetic current slots. Therefore, the antenna radiates omnidirectionally and is not compromised by the coupling. We note that it would be possible to design a seamless tuning without gaps between consecutive bands, although with trade-offs in the tuning independence between adjacent bands.

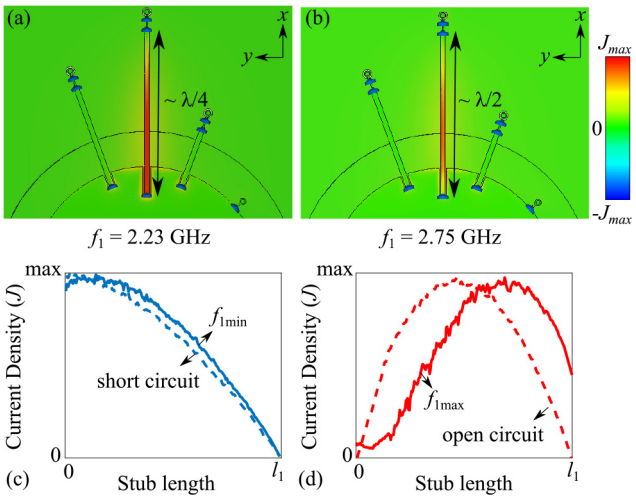

FIGURE 9. Simulated surface current distribution when frequency of the first band f_1 tuned to the (a) minimum and (b) maximum. (c, d) Normalized surface current density along the length of the stub for the case shown in (a, b), respectively. The blue and red solid lines illustrate the simulated surface current density when the capacitance of the varactors are tuned to the minimum and maximum, respectively. The dotted lines depict the simulated surface current density when the varactors are substituted with short circuit (blue) and open circuit (red) for comparison.

D. SURFACE CURRENT DISTRIBUTION

Figure 9 shows two examples of surface current distributions of the active tuning stub at the lowest band. In Fig. 9(a) the varactor on the longest stub is biased with the minimum tuning voltage $V_1 = 0$, resulting in a capacitance of 1.30 pF. At this minimum tuning frequency $f_1 = 2.23$ GHz, the current density in the stub is depicted in Fig. 9(c) with the maximum approximately at the beginning of the stub (patch edge) and the minimum at its end. This suggests that the stub works equivalently as an opened $\lambda/4$ transmission line which effectively creates a short near the edge of the circular patch. On the other hand, for the case when f_1 is tuned to the maximum of 2.75 GHz with the varactor capacitance set to 0.15 pF, the current density is shown in Fig. 9(b) and Fig. 9(d). In this condition, the location where the stub has the maximum current density is shifted toward the center, indicating that the impedance at the beginning of the stub is increased due to the smaller varactor capacitance. The varactor can be considered as a loaded impedance at the antenna aperture as explained in [31]. The variation of the impedance affects the fringing field and thus the resonance frequency is shifted. Simulated surface current distributions with a short and an open circuits are included as dotted lines in Fig. 9(c) and Fig. 9(d). They are added to show comparisons with the two varactors extreme scenarios.

E. RADIATION PATTERNS

The normalized simulated and measured radiation patterns at the minimum and maximum tuning frequencies for each of the three bands are depicted in Fig. 10. A good qualitative agreement is observed between simulation and measurement. In the azimuth *xy*-plane, monopole-like radiation patterns are obtained at all sweeping frequencies, whereas in the elevation

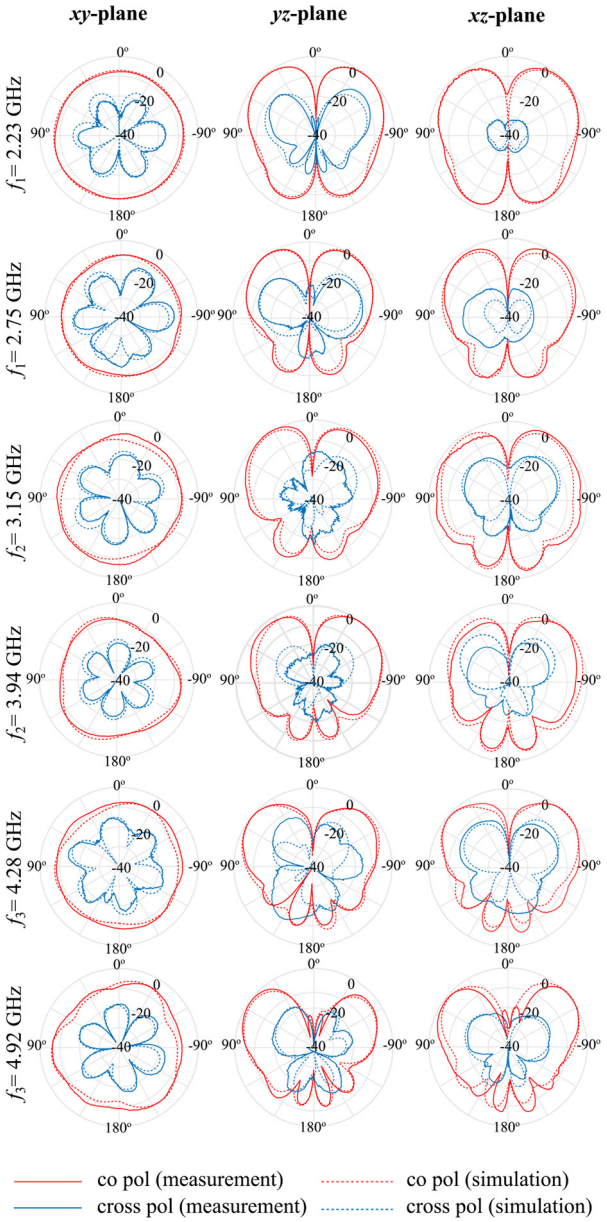

FIGURE 10. Normalized radiation patterns of the triple-band reconfigurable low-profile monopole antenna at the minimum and maximum tuning frequencies for the first, second, and third bands.

yz-plane, the radiation patterns are conical as a result of the finite ground plane similarly as monopole antennas that were proposed in [1], [3]–[5], [40]. The omni-directional radiation patterns are required for applications where a large coverage in the azimuthal plane is needed. It is emphasized that the co- and cross-polarizations in the omnidirectional *xy*-plane patterns are measured at the horizon, i.e., $\theta = 90°$. Despite that the maximum of the conical patterns occurs above the horizon, the measurement in this azimuthal plane provides a good indication of the omnidirectionality of the antenna. It is observed that at the highest tuning frequency in the second and the third bands, the patterns in the *xy*-plane become more directive towards the active shorting

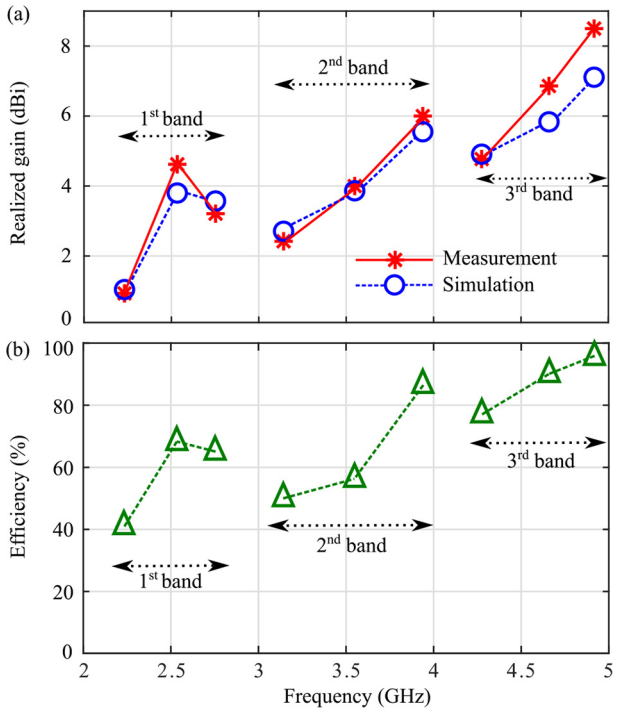

FIGURE 11. Gain and efficiency of the antenna. (a) Realized gain of the triple-band reconfigurable antenna across the three tuning ranges. (b) Simulated total efficiency of the triple-band reconfigurable antenna across the three tuning ranges.

stubs. Ideally, from image theory it is known that the electric current flows over the stubs is canceled out by the reflected image from the ground plane. As a result there should be no substantial net radiation from the stubs. However, for these two particular tuning conditions, the separation between the antenna and the ground plane is becoming sufficiently large. As a result, parasitic radiations originating from the stubs can be observed. The stubs then can be seen as electric dipoles at a non-negligible distance above the ground plane, and together with the slots they contribute to the total radiation pattern. This pattern degradation should be considered and might set a limitation of the proposed design concept for further extension into a higher number of bands.

F. ANTENNA EFFICIENCY AND GAIN

The measured and simulated realized gain profiles are compared in Fig. 11(a). The gain is generally increasing with frequency. For the first band, the measured gain is between 0.93 and 4.62 dBi, whereas the second one is between 2.42 and 6.00 dBi, and the third one spans from 4.77 to 8.50 dBi. At higher frequencies, the patterns become more conical because the ground plane is electrically larger and this leads to a higher gain. The simulated radiation efficiency of the antenna is displayed in Fig. 11(b). In the first band, the efficiency ranges from 40% to 70%, for the second band the efficiency is between 50% to 87%, and increases from 77% to 96% in the third band. The lower antenna efficiency is mostly because of the higher loss in the internal resistances of the varactors. In the lowest frequency, a higher current flows through the varactors when the capacitance is at the highest value (1.30 pF). The capacitance drops by one order of magnitude to 0.15 pF at the highest tuning. This condition resembles closely as an open circuit, resulting in almost no current flowing through the varactors. Due to the limitation of our facility, the efficiency cannot be measured directly. However, the actual radiation efficiency of the antenna is expected to be close to the simulated one, considering the general agreement between the simulated and measured realized gains. Nevertheless, it is noted that discrepancies of up to 1 dB observed in the measured and simulated gains are due to the imperfect measurement as well as the non-ideal chamber conditions. The efficiency can be increased by choosing varactors with a lower intrinsic resistance. However, this may come with a trade-off of a limited tuning range.

G. COMPARISON WITH EXISTING DESIGNS

Table 1 shows a comparison on the performance of some typical reported antennas with frequency reconfigurability in multi-bands where λ_{min} is the free-space wavelength at the minimum operation frequency of each antenna. The antenna reported in [21] offered the largest number of independent tunable bands among the others. However, the highest band has a very small tuning range of 3%. In addition, the design did not consider the stability and nature of the radiation patterns. The shape of the patterns was undefined. Among the published designs with broadside patterns [12], [22], [24], [25], the antenna in [25] featured the highest number of tunable bands. They proposed three independent tuning frequencies and the tuning ranges were measured for more than 34% for each band. Nonetheless, these ranges were calculated based on minimum −6 dB bandwidth. The proposed design is more suitable to be compared with antennas that also radiate omnidirectionally as in [14] and [34]. Between these two dual-band antennas, only the antenna in [14] can be tuned independently. Compared to these designs, the antenna in this paper demonstrates a larger number of tunable bands with a higher measured maximum gain. In terms of size, this proposed antenna is among the largest in the list. However, the antenna is low-profile with only 4.32 mm (0.032 λ_{min}) of height and can be easily integrated onto a flat surface such as rooftop or cartop for future applications. The number of diodes used in this proposed antenna is comparable to [14]. In that work, two sets of four varactors were used to create a dual-band reconfigurable antenna. Meanwhile, this works uses three sets of three varactors to create three operation bands. It is understandable that these relatively large number of components can increase the antenna cost. Nonetheless, in view of the achieved advanced antenna features such as independent tunability, the number of varactors might not be a critical problem for the design. It is also noted that several published designs have utilized stub-loaded antenna structures [31], [41], [42]. Nevertheless, none of these works uses a concept of multi-length shorting stubs to create different magnetic current sources, which is the core of the monopolar multi-band antenna proposed in this article.

TABLE 1. Performance comparison between presented design and published frequency reconfigurable multi-band antennas.

Ref.	No. of Bands (Tunable)	Tunability (%)	Independent	Pattern	Max Gain (dBi)	Center Frequency (GHz)	Size	No. of Diodes
[21]	5 (4)	23.5, 10.3, 13.5, n.a., 3	Yes	Undefined	-4.2, 0.95, 1.19, 0.92, 1	1.04, 1.65, 2.12, 2.4, 2.95	$0.14\lambda_{min}$ x $0.14\lambda_{min}$	4
[22]	2 (1)	n.a., 29.2	No	Broadside	7, 6.8	2.24, 3.8	$0.74\lambda_{min}$ x $0.74\lambda_{min}$	1
[24]	2 (2)	n.a.	No	Broadside	n.a., 2.7	1.58, 2.45	$0.19\lambda_{min}$ x $0.08\lambda_{min}$	2
[12]	2 (2)	19.7, 51.3	Yes	Broadside	1.2, 1.8	1.22, 2.34	$0.4\lambda_{min}$ x $0.55\lambda_{min}$	2
[25]	3 (3)	58.8, 85.7, 34.7 [a]	Yes	Broadside	-2.06, -0.55, 0.31	0.85, 1.75, 2.3	$0.1\lambda_{min}$ x $0.2\lambda_{min}$	3
[34]	2 (2)	11, 29.2	No	Monopolar	2.37, -0.41	2.4, 3.6	$0.04\lambda_{min}$ x $0.08\lambda_{min}$	1
[14]	2 (2)	31, 22	Yes	Monopolar	3.5, 5.5	0.9, 1.7	$0.71\lambda_{min}$ x $0.71\lambda_{min}$	8
This work	3 (3)	22.8, 22.8, 16.7	Yes	Monopolar	4.62, 6, 8.5	2.51, 3.56, 4.62	$1.1\lambda_{min}$ x $1.1\lambda_{min}$	9

[a] −6 dB bandwidth

IV. CONCLUSION

In this article, a frequency-reconfigurable low-profile monopolar antenna with independently tunable bands has been presented. The multi-band antenna is based on the concept of a center-fed patch with shortings to create independent magnetic current loops sharing the same thin aperture. Groups of quarter-wavelength stubs are located at the patch edge with each set of stubs functioning as equivalent shortings at a particular frequency. Frequency-reconfigurability is achieved by placing sets of varactor diodes between the patch and the stubs. The implementation of the principle into a triple-band design demonstrates center operation frequencies at 2.51, 3.56, and 4.62 GHz with −10 dB independent tuning ranges of 22.8%, 22.8%, and 16.7%, respectively. The number of bands is limited by the stub-stub and stub-slot couplings, and the electrical separation between the patch and ground plane. For the radiation patterns, the antenna radiates omnidirectionally with vertical polarization across the tuning ranges, indicating that the magnetic current slots remain the predominant radiating sources. All these results suggest that the proposed antenna design is promising for advanced applications that require independent reconfigurability in multi-band operation, such as software-defined radio or carrier aggregation systems. The advantages include simple antenna geometry, ease of fabrication, and low profile.

ACKNOWLEDGMENT

The authors would like to thank A. O'Brien, N. Itsumi, and D. Di Giacomo for their help in the fabrication of the antennas.

REFERENCES

[1] H. Nakano, H. Iwaoka, K. Morishita, and J. Yamauchi, "A wideband low-profile antenna composed of a conducting body of revolution and a shorted parasitic ring," *IEEE Trans. Antennas Propag.*, vol. 56, no. 4, pp. 1187–1192, Apr. 2008.

[2] Y. M. Pan, S. Y. Zheng, and B. J. Hu, "Wideband and low-profile omnidirectional circularly polarized patch antenna," *IEEE Trans. Antennas Propag.*, vol. 62, no. 8, pp. 4347–4351, Aug. 2014.

[3] K. Ghaemi and N. Behdad, "A low-profile, vertically polarized ultra-wideband antenna with monopole-like radiation characteristics," *IEEE Trans. Antennas Propag.*, vol. 63, no. 8, pp. 3699–3705, Aug. 2015.

[4] N. Nguyen-Trong, A. Piotrowski, T. Kaufmann, and C. Fumeaux, "Low-profile wideband monopolar UHF antennas for integration onto vehicles and helmets," *IEEE Trans. Antennas Propag.*, vol. 64, no. 6, pp. 2562–2568, Jun. 2016.

[5] A. A. Omar and Z. Shen, "A compact and wide-band vertically polarized monopole antenna," *IEEE Trans. Antennas Propag.*, vol. 67, no. 1, pp. 626–631, Jan. 2019.

[6] H. Boudaghi, M. Azarmanesh, and M. Mehranpour, "A frequency-reconfigurable monopole antenna using switchable slotted ground structure," *IEEE Antennas Wireless Propag. Lett.*, vol. 11, pp. 655–658, 2012.

[7] T. Li, H. Zhai, X. Wang, L. Li, and C. Liang, "Frequency-reconfigurable bow-tie antenna for Bluetooth, WiMAX, and WLAN applications," *IEEE Antennas Wireless Propag. Lett.*, vol. 14, pp. 171–174, 2015.

[8] Y. Tawk, A. El-Amine, S. Saab, J. Costantine, F. Ayoub, and C. G. Christodoulou, "A software-defined frequency-reconfigurable meandered printed monopole," *IEEE Antennas Wireless Propag. Lett.*, vol. 17, no. 2, pp. 327–330, Feb. 2018.

[9] I. Kim and Y. Rahmat-Samii, "RF-MEMS switchable slot patch antenna integrated with bias network," *IEEE Trans. Antennas Propag.*, vol. 59, no. 12, pp. 4811–4815, Dec. 2011.

[10] C.-Y. Chiu, J. Li, S. Song, and R. D. Murch, "Frequency-reconfigurable pixel slot antenna," *IEEE Trans. Antennas Propag.*, vol. 60, no. 10, pp. 4921–4924, Oct. 2012.

[11] D. E. Anagnostou, M. T. Chryssomallis, B. D. Braaten, J. L. Ebel, and N. Sepúlveda, "Reconfigurable UWB antenna with RF-MEMS for on-demand WLAN rejection," *IEEE Trans. Antennas Propag.*, vol. 62, no. 2, pp. 602–608, Feb. 2014.

[12] N. Behdad and K. Sarabandi, "Dual-band reconfigurable antenna with a very wide tunability range," *IEEE Trans. Antennas Propag.*, vol. 54, no. 2, pp. 409–416, Feb. 2006.

[13] N. Nguyen-Trong, L. Hall, and C. Fumeaux, "A frequency- and pattern-reconfigurable center-shorted microstrip antenna," *IEEE Antennas Wireless Propag. Lett.*, vol. 15, pp. 1955–1958, 2016.

[14] N. Nguyen-Trong, A. Piotrowski, and C. Fumeaux, "A frequency-reconfigurable dual-band low-profile monopolar antenna," *IEEE Trans. Antennas Propag.*, vol. 65, no. 7, pp. 3336–3343, Jul. 2017.

[15] S. N. M. Zainarry, N. Nguyen-Trong, and C. Fumeaux, "A frequency- and pattern-reconfigurable two-element array antenna," *IEEE Antennas Wireless Propag. Lett.*, vol. 17, no. 4, pp. 617–620, Apr. 2018.

[16] S. J. Chen, D. C. Ranasinghe, and C. Fumeaux, "A robust snap-on button solution for reconfigurable wearable textile antennas," *IEEE Trans. Antennas Propag.*, vol. 66, no. 9, pp. 4541–4551, Sep. 2018.

[17] C.-H. Wu and T.-G. Ma, "Pattern-reconfigurable self-oscillating active integrated antenna with frequency agility," *IEEE Trans. Antennas Propag.*, vol. 62, no. 12, pp. 5992–5999, Dec. 2014.

[18] M. S. Alam and A. Abbosh, "A compact reconfigurable antenna with wide tunable frequency and 360° beam scanning," *IEEE Antennas Wireless Propag. Lett.*, vol. 18, no. 1, pp. 4–8, Oct. 2019.
[19] H. Li, J. Xiong, Y. Yu, and S. He, "A simple compact reconfigurable slot antenna with a very wide tuning range," *IEEE Trans. Antennas Propag.*, vol. 58, no. 11, pp. 3725–3728, Nov. 2010.
[20] P.-L. Chi, R. Waterhouse, and T. Itoh, "Compact and tunable slot-loop antenna," *IEEE Trans. Antennas Propag.*, vol. 59, no. 4, pp. 1394–1397, Apr. 2011.
[21] H. F. Abutarboush, R. Nilavalan, S. W. Cheung, and K. M. Nasr, "Compact printed multiband antenna with independent setting suitable for fixed and reconfigurable wireless communication systems," *IEEE Trans. Antennas Propag.*, vol. 60, no. 8, pp. 3867–3874, Aug. 2012.
[22] A. Khidre, F. Yang, and A. Z. Elsherbeni, "A patch antenna with a varactor-loaded slot for reconfigurable dual-band operation," *IEEE Trans. Antennas Propag.*, vol. 63, no. 2, pp. 755–760, Feb. 2015.
[23] Y. Cai, K. Li, Y. Yin, S. Gao, W. Hu, and L. Zhao, "A low-profile frequency reconfigurable grid-slotted patch antenna," *IEEE Access*, vol. 6, pp. 36305–36312, 2018.
[24] C. Hung and T. Chiu, "Dual-band reconfigurable antenna design using slot-line with branch edge," *IEEE Trans. Antennas Propag.*, vol. 63, no. 2, pp. 508–516, Feb. 2015.
[25] Q. Bai, R. Singh, K. L. Ford, T. O'Farrell, and R. J. Langley, "An independently tunable tri-band antenna design for concurrent multi-band single chain radio receivers," *IEEE Trans. Antennas Propag.*, vol. 65, no. 12, pp. 6290–6297, Dec. 2017.
[26] P. Qin, A. R. Weily, Y. J. Guo, T. S. Bird, and C. Liang, "Frequency reconfigurable quasi-Yagi folded dipole antenna," *IEEE Trans. Antennas Propag.*, vol. 58, no. 8, pp. 2742–2747, Sep. 2010.
[27] Y. Cai, Y. J. Guo, and T. S. Bird, "A frequency reconfigurable printed Yagi–Uda dipole antenna for cognitive radio applications," *IEEE Trans. Antennas Propag.*, vol. 60, no. 6, pp. 2905–2912, Jun. 2012.
[28] T. Li, H. Zhai, L. Li, and C. Liang, "Frequency-reconfigurable bow-tie antenna with a wide tuning range," *IEEE Antennas Wireless Propag. Lett.*, vol. 13, pp. 1549–1552, 2014.
[29] M. N. M. Kehn, Ò. Quevedo-Teruel, and E. Rajo-Iglesias, "Reconfigurable loaded planar inverted-F antenna using varactor diodes," *IEEE Antennas Wireless Propag. Lett.*, vol. 10, pp. 466–468, 2011.
[30] S. Sam and S. Lim, "Compact frequency-reconfigurable half-mode substrate-integrated waveguide antenna," *IEEE Antennas Wireless Propag. Lett.*, vol. 12, pp. 951–954, 2013.
[31] N. Nguyen-Trong, T. Kaufmann, L. Hall, and C. Fumeaux, "Analysis and design of a reconfigurable antenna based on half-mode substrate-integrated cavity," *IEEE Trans. Antennas Propag.*, vol. 63, no. 8, pp. 3345–3353, Aug. 2015.
[32] A. Tariq and H. Ghafouri-Shiraz, "Frequency-reconfigurable monopole antennas," *IEEE Trans. Antennas Propag.*, vol. 60, no. 1, pp. 44–50, 2012.
[33] L. Ge and K.-M. Luk, "Frequency-reconfigurable low-profile circular monopolar patch antenna," *IEEE Trans. Antennas Propag.*, vol. 62, no. 7, pp. 3443–3449, Jul. 2014.
[34] R. O. Ouedraogo, J. Tang, K. Fuchi, E. J. Rothwell, A. R. Diaz, and P. Chahal, "A tunable dual-band miniaturized monopole antenna for compact wireless devices," *IEEE Antennas Wireless Propag. Lett.*, vol. 13, pp. 1247–1250, 2014.
[35] T. Kaufmann and C. Fumeaux, "Low-profile magnetic loop monopole antenna based on a square substrate-integrated cavity," *Int. J. Antennas Propag.*, vol. 2015, Jan. 2015, Art. no. 694385.
[36] K. Paramayudha, S. J. Chen, W. Withayachumnankul, and C. Fumeaux, "Low-profile monopole antenna with via-less shorting," in *Proc. Aust. Microw. Symp. (AMS)*, 2018, pp. 11–12.
[37] D. G. Chen and K. W. Eccleston, "Substrate integrated waveguide with corrugated wall," in *Proc. Asia–Pac. Microw. Conf.*, 2008, pp. 1–4.
[38] C. A. Balanis, *Antenna Theory: Analysis and Design*, 3rd ed. Hoboken, NJ, USA: Wiley-Intersci., 2005.
[39] T. P. Lee, "Evaluation of voltage dependent series resistance of epitaxial varactor diodes at microwave frequencies," *IEEE Trans. Electron Devices*, vol. ED-12, no. 8, pp. 457–470, Aug. 1965.
[40] M. Niroo-Jazi and T. A. Denidni, "A new triple-band circular ring patch antenna with monopole-like radiation pattern using a hybrid technique," *IEEE Trans. Antennas Propag.*, vol. 59, no. 10, pp. 3512–3517, Oct. 2011.
[41] M. S. Alam and A. M. Abbosh, "Beam-steerable planar antenna using circular disc and four pin-controlled tapered stubs for WiMAX and WLAN applications," *IEEE Antennas Wireless Propag. Lett.*, vol. 15, pp. 980–983, 2016.
[42] P. Qin, Y. J. Guo, Y. Cai, E. Dutkiewicz, and C. Liang, "A reconfigurable antenna with frequency and polarization agility," *IEEE Antennas Wireless Propag. Lett.*, vol. 10, pp. 1373–1376, 2011.

KEN PARAMAYUDHA received the B.E. degree in electrical engineering from the Bandung Institute of Technology, Indonesia, in 2009, and the M.Phil. degree in electrical and electronic engineering from the University of Adelaide, Australia, in 2019. Since 2014, he has been working as a Research Associate with the Research Center for Electronics and Telecommunication, Indonesian Institute of Sciences (PPET-LIPI). In 2017, he received the Riset-PRO Scholarship from the Indonesian Ministry of Research, Technology, and Higher Degree Education to continue his master's study with the University of Adelaide. He joined the School of Electrical and Electronic Engineering as a research student in the area of applied electromagnetics. His current research interests include reconfigurable antennas and microwave devices. During his candidature, he was the finalist of the Best Student Paper Award at Australian Microwave Symposium in 2018. He was a recipient of the Best Poster Presentation Award at Indonesia–Japan Workshop on Antennas and Wireless Technology in 2019.

SHENGJIAN JAMMY CHEN (Member, IEEE) received the B.E. degree in information engineering from the Guangdong University of Technology, Guangzhou, China, in 2003, and the M.E. and Ph.D. degrees in electrical and electronic engineering from the University of Adelaide, Australia, in 2013 and 2017, respectively. Since June 2017, he has been working as a Postdoctoral Researcher and a Lecturer with the School of Electrical and Electronic Engineering, University of Adelaide. His current research interests include RFID-based wearable applications, leaky wave antennas, microwave absorbers, as well as wearable and reconfigurable electromagnetic structures based on novel conductive materials, such as graphene, conductive polymers, and conductive fabrics. He received a number of scholarships, including the Australian Postgraduate Award in 2013 and the 2015 Simon Rockliff Scholarship for Outstanding Mentorship. He was a recipient of a number of awards, including the Young Scientist Best Paper Award at the International Conference on Electromagnetics in Advanced Applications (ICEAA) in 2015, the Young Scientist Best Paper Award and the Travel Bursary Award at the ICEAA in 2016, the Honorable Mention at IEEE AP-S Symposium on Antennas and Propagation (APS/URSI) in 2017, and the CST University Publication Award in 2017. He serves as a reviewer of some prestigious journals, including the IEEE TRANSACTIONS ON ANTENNAS AND PROPAGATION, the IEEE TRANSACTIONS ON MICROWAVE THEORY AND TECHNIQUES, the IEEE ANTENNAS AND WIRELESS PROPAGATION LETTERS, the IEEE TRANSACTIONS ON BIOMEDICAL CIRCUITS AND SYSTEMS, IEEE ACCESS, and *Electronics Letters*. He has also been serving as the Chair of the IEEE South Australia Joint Chapter on Microwave Theory and Techniques & Antennas and Propagation since 2019.

THOMAS KAUFMANN (Member, IEEE) received the M.Sc. degree in electrical engineering and information technology from ETH Zürich, Zürich, Switzerland, in 2007, and the Ph.D. degree from the Laboratory for Electromagnetic Fields and Microwave Electronics (IFH), ETH Zürich in 2011. From 2011 to 2015, he was a Lecturer and a Postdoctoral Researcher with the School of Electrical and Electronic Engineering, University of Adelaide, Australia. He is with u-blox AG, Switzerland, as a Principal Engineer of modeling & antennas. His research interests include GNSS antennas and propagation effects, UWB ranging and localization technologies, electromagnetic structures made from conductive polymers and fabrics, substrate-integrated antennas and computational electromagnetics in the microwave, and THz region. He was a recipient of the Best Symposium Paper Award at the 2012 Asia–Pacific International Symposium on Electromagnetic Compatibility and 17ẽme Colloque International et Exposition sur la Compatibilité ÉlectroMagnétique in 2014, the supervisor of a number of recipients of Best Paper Awards at the International Workshop on Antennas and Propagation in 2014, and the 2014 Australian Microwave Symposium Best Student Paper Award. He served as the Chair of the South Australian IEEE Joint AP/MTT Chapter from 2013 to 2015.

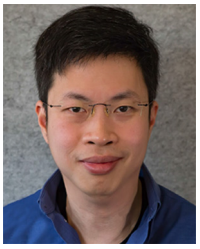

WITHAWAT WITHAYACHUMNANKUL (Senior Member, IEEE) received the bachelor's and master's degrees in electronic engineering from the King Mongkut's Institute of Technology Ladkrabang, Thailand, in 2001 and 2003, respectively, and the Doctoral degree in electrical engineering with a special commendation from the University of Adelaide, Australia, in 2010. In 2015, he was a Research Fellow with the Japan Society for the Promotion of Science, Tokyo Institute of Technology. He has been a Visiting Researcher with Osaka University in recent years. He is currently an Associate Professor and the Postgraduate Coordinator with the University of Adelaide, and the Founding Leader of the Terahertz Engineering Laboratory. He has authored and coauthored more than 80 journal publication, and has supervised six Ph.D. students to completion, all with commendation. His research interests include terahertz waveguides, antennas, radar, communications, and metrology. In 2010, he was awarded a 3-year Australian Research Council (ARC) Australian Postdoctoral Fellowship. He is a recipient of the IRMMW-THz Society Young Scientist Award in 2020. From 2017 to 2018, he was the Chair of the IEEE South Australia Joint Chapter on Microwave Theory and Techniques & Antennas and Propagation. In recent years, he is a lead investigator for three ARC grants, totalling to over AUD 1M. He currently serves as an Associate Editor for the IEEE TRANSACTIONS ON TERAHERTZ SCIENCE AND TECHNOLOGY.

CHRISTOPHE FUMEAUX (Fellow, IEEE) received the Diploma and Ph.D. degrees in physics from ETH Zürich, Switzerland, in 1992 and 1997, respectively. From 1998 to 2000, he was a Postdoctoral Researcher with the School of Optics, University of Central Florida, Orlando. In 2000, he joined the Swiss Federal Office of Metrology, Bern, Switzerland, as a Scientific Staff Member. From 2001 to 2008, he was a Research Associate and a Lecturer with the Laboratory for Electromagnetic Fields and Microwave Electronics, ETH Zürich. Since 2008, he has been with the University of Adelaide, Australia, where he is currently a Professor with the School of Electrical and Electronic Engineering. His current main research interests concern antenna engineering, THz technology, and the application of RF design principles to optical micro/nano-structures. He was the recipient of the ETH Medal for his doctoral dissertation, the 2018 Edward E. Altshuler Prize, the 2014 IEEE SENSORS JOURNAL, the 2004 ACES Journal Best Paper Awards, the Best Conference Paper Awards at the 2012 Asia–Pacific International Symposium on Electromagnetic Compatibility in 2012, the 17th Colloque International sur la Compatibilité Electromagnétique in 2014, and the University of Adelaide Stephen Cole the Elder Award for Excellence in Higher Degree by Research Supervisory Practice in 2018. More than ten of his students have received student awards with joint papers at IEEE conferences. From 2011 to 2015, he was a Future Fellow of the Australian Research Council. He served as an Associate Editor for the IEEE TRANSACTIONS ON MICROWAVE THEORY AND TECHNIQUES from 2010 to 2013. From 2013 to 2016, he served as a Senior Associate Editor and later as an Associate Editor-in-Chief for the IEEE TRANSACTIONS ON ANTENNAS AND PROPAGATION. Since March 2017, he has been serving as the Editor-in-Chief for the IEEE ANTENNAS AND WIRELESS PROPAGATION LETTERS.